Electroimpulse Deicing: Electrodynamic Solution by Discrete Elements

W. D. Bernhart* and R. L. Schrag†
Wichita State University, Wichita, Kansas

This paper describes a technique for analyzing the electrodynamic phenomena associated with electroimpulse deicing. The analysis is done in the time domain and utilizes a discrete element formulation concept expressed in state variable form. Calculated results include coil current, eddy currents in the target (aircraft leading-edge skin), pressure distribution on the target, and total force and impulse on the target. Typical results are presented and described. Some comparisons are made between calculated and experimental results and also between calculated values from other theoretical approaches. Application to the problem of a nonrigid target is treated briefly.

Introduction

THERE has been considerable interest recently in computational procedures applicable to the design of electroimpulse (EIDI) systems for aircraft ice protection. An essential part of the total design process is the determination of the mechanical driving force that results from the transient current in the impulse coil. The major emphasis in available literature has been the calculation of mechanical impulse strength. Bowley et al.[1] and Lewis[2] have described a procedure for calculating the mechanical impulse on a flat metal plate due to a circular cylindrical coil carrying either a half or full cycle of idealized damped oscillatory current. Henderson[3] included a model of the EIDI circuit behavior and calculated the temporal characteristics of the mechanical driving force. This procedure has proved to be computationally intensive.

Bernhart and Gien[4] have analyzed the mechanical response of a semicylindrical structure excited by an impulse coil and have concluded that the dynamic response of the shell is sensitive to the shape of the mechanical pressure distribution as well as its temporal dependence. This realization provided the motive for developing a new computational procedure that will provide the detailed pressure and time behavior of the mechanical impulse in a computationally efficient manner.

The Model

The basic EIDI system is displayed in Fig. 1, with the capacitor charging and SCR firing circuits omitted. In normal operation, energy is first stored on the capacitor by a charging circuit. Then the SCR is fired, causing a large transient current in the impulse coil and induced eddy currents in the target. Diode D in Fig. 1 prevents reverse charging of the capacitor. The target experiences a sharp mechanical pulse directed away from the coil. The coil is mounted on a rigid base and is assumed to be circularly wound with rectangular wire, starting from some inner radius. The thickness of the coil is the wider dimension of the rectangular wire, and both the coil and target are assumed to be flat. In practice, several coils may be pulsed simultaneously with either series or parallel arrangements. The model further assumes that all coils in multiple coil operation are identical.

Figure 2 is an equivalent circuit with some nomenclature illustrated. The feed cable is modeled as a series resistance and inductance. Symbol E represents the voltage across the terminals of one coil, while I is the current in this coil. Symbols n_s and n_p represent the number of series or parallel coils, respectively; the default values for a single coil are unity. The SCR is assumed to be an ideal switch. In the conduction state, the diode is assumed to have a constant voltage drop denoted as V_d. This diode goes into conduction at time t_x, as shown in Fig. 2, and the initial capacitor voltage is denoted as V_o. The circuit equation may be written as

$$v_c - R_w(n_pI) - L_w(n_pI) = n_sE \tag{1}$$

where

$$v_c = v_0 - \frac{1}{C}\int_0^t n_pI\,dt \quad (t < t_x) \tag{2}$$

$$v_c = -V_d \quad (t > t_x) \tag{3}$$

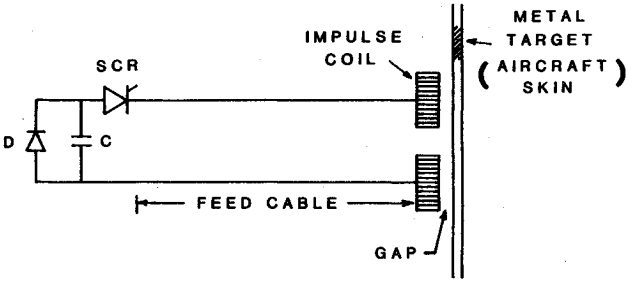

Fig. 1 Basic EIDI system.

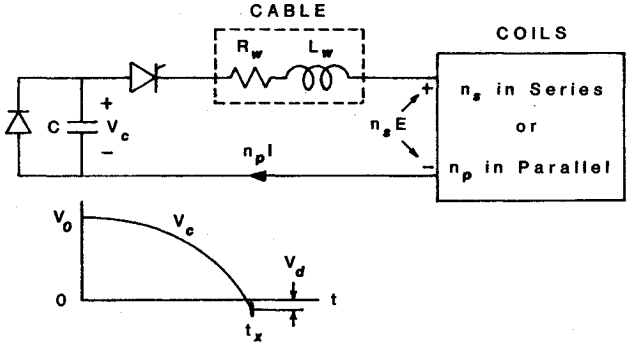

Fig. 2 Equivalent circuit.

Presented as Paper 88-0018 at the AIAA 26th Aerospace Sciences Meeting, Reno, NV, Jan. 11–14, 1988; received March 10, 1988; revision received April 7, 1988.

*Professor of Aeronautical Engineering. Senior Member AIAA.
†Professor of Electrical Engineering.

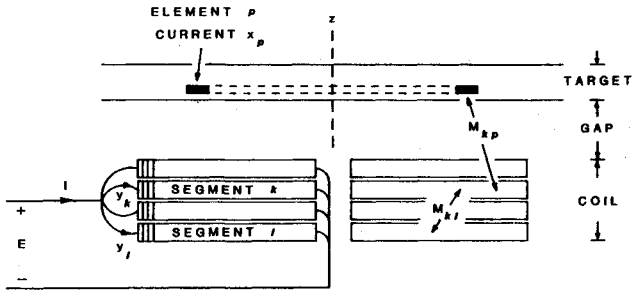

Fig. 3 Coil and target discretization.

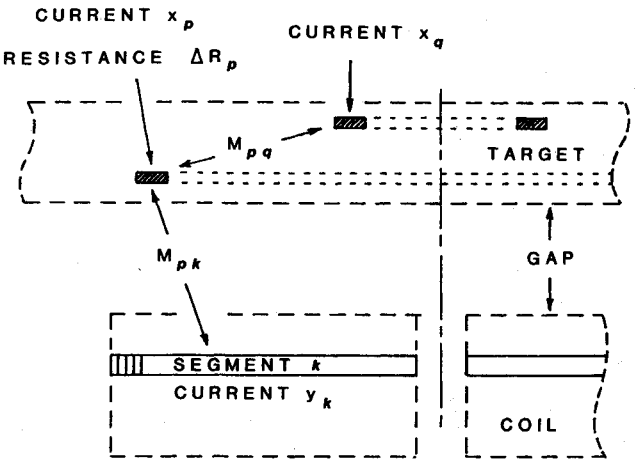

Fig. 4 Illustration for formulating the target equation.

Figure 3 illustrates the manner in which the coil and target are discretized. The coil is subdivided equally in thickness, and each subdivision is called a segment. Segment k carries the current y_k, while the total coil current is the sum of the individual segment currents. The target is subdivided into coaxial rings with rectangular cross sections. These are identified as elements. Target element p has the eddy current x_p. The coil segments have self inductance, M_{kk}, and mutual inductances to all other segments, M_{kl}. Coil segments also have mutual inductances to the target elements, M_{kp}. The coil equation has the form

$$E_k = y_k\,\Delta R_c + \sum_l M_{kl}\dot{y}_l + \sum_p M_{kp}\dot{x}_p \tag{4}$$

where ΔR_c is the dc resistance of the coil segment.

The equation governing the target currents may be formulated with the aid of Fig. 4. Designating the dc resistance of target element p as ΔR_p and the mutual inductance between elements p and q as M_{pq}, then the target equation is

$$x_p\,\Delta R_p + \sum_k M_{pk}\dot{y}_k + \sum_q M_{pq}\dot{x}_q = 0 \tag{5}$$

Equations (1), (4), and (5) may be solved simultaneously to establish the currents in the various coil segments and target elements. Once these currents are known, the target pressure may be calculated. The z component of force on target element p is

$$F_{zp} = -2\pi r_p x_p\left[\sum_k B_{rpk} + \sum_q B_{rpq}\right] \tag{6}$$

where r_p is the mean radius of p, B_{rpk} is the radial component of the magnetic flux density at element p due to coil k, and B_{rpq} is the radial component of magnetic flux density at element p due to target element q. These flux densities are calculated by the formulas

$$B_{rpk} = -\frac{y_k}{2\pi r_p}\frac{\partial M_{pk}}{\partial z} \tag{7}$$

$$B_{rpq} = -\frac{x_q}{2\pi r_p}\frac{\partial M_{pq}}{\partial z} \tag{8}$$

The normal pressure on the target may then be found from

$$P_z(r) = \frac{1}{2\pi r_p\,\Delta r}\sum_{\substack{\text{over}\\ h}} F_{zp} \tag{9}$$

where Δr is the radial range of the elements and h is the target thickness.

A radially directed body force is also present within the target, and it may be of interest in the structural dynamic response problem. The radial force produced within the radial range Δr is

$$\Delta F_r(r) = \sum_{\substack{\text{over}\\ h}} 2\pi r_p x_p\left[\sum_k B_{zpk} + \sum_q B_{zpq}\right] \tag{10}$$

where

$$B_{zpk} = \frac{y_k}{2\pi r_p}\frac{\partial M_{pk}}{\partial r} \tag{11}$$

$$B_{zpq} = \frac{x_q}{2\pi r_p}\frac{\partial M_{pq}}{\partial r} \tag{12}$$

State Variable Formulation and Solution

It may be shown that Eqs. (1), (2), (4), and (5) may be combined into the matrix equation

$$\begin{bmatrix} n_s M_{TT} & n_s M_{TC} & 0 \\ n_s M_{CT} & n_s M_{CC} + n_p L_w & 0 \\ 0 & 0 & -\dfrac{C}{n_p} \end{bmatrix}\begin{Bmatrix}\dot{x}\\ \dot{y}\\ \dot{v}_c\end{Bmatrix} + \begin{bmatrix} n_x\,\Delta R_T & 0 & 0 \\ 0 & n_p R_w + n_s\,\Delta R_c & (-1) \\ 0 & (-1) & 0 \end{bmatrix}\begin{Bmatrix} x\\ y\\ v_c\end{Bmatrix} = \begin{Bmatrix} 0\\ 0\\ \dfrac{-CV_0\delta(t)}{n_p}\end{Bmatrix} \tag{13}$$

where the submatrices have the following meanings:

$\{M_{TT}\}$ The self and mutual inductance of and between all discrete target elements. A square symmetric array of order N_T, the total number of target elements.

$\{M_{CC}\}$ The self and mutual inductance of and between all coil segments. A square symmetric array of order N_C, the total number of coil segments.

$\{M_{TC}\}$ The mutual inductance between the N_T target elements and N_C coil segments. This array is of order (N_T, N_C).

$\{M_{CT}\}$ The transpose of $\{M_{TC}\}$.

$\{L_w\}$ The inductance of the external circuit. A square array of order N_C, with all elements equal to the scalar inductance L_w.

$\{R_w\}$ The resistance of the external circuit. A square array of order N_C, with all elements equal to the scalar resistance R_w.

$\{R_T\}$ The set of resistance values for each discrete target element. A square diagonal array of order N_T.

$\{\Delta R_C\}$ The set of resistance values for each coil segment. A square diagonal array of order N_C.

$\{C\}$ The scalar capacitance.

Equation (13) has the following state model form:

$$[A]\{\dot{Z}\} + [B]\{Z\} = \{f(t)\}, \quad \{Z(0)\} = 0 \tag{14}$$

where the state vector $\{Z\}$ consists of the following variables:

$\{X\}$ Eddy currents in the N_T discrete target elements.
$\{Y\}$ Currents in the N_C coil segments.
$\{v_c\}$ Capacitor voltage.

Thus, the total order of the system is given by

$$N = N_T + N_c + 1 \tag{15}$$

An eigensolution is performed on the state model given by Eq. (14) by employing a standard discrete eigenexpansion. The eigensolution may be performed by finding the inverse of either array $[A]$ or $[B]$. Array $[A]$ is composed of self and mutual inductance terms for both the target and coil with the self inductance terms distributed along the diagonal. The mutual inductance of a near-diagonal element is nearly equal to the self inductance in numerical value. This creates a poorly conditioned matrix for inversion purposes. Conversely, the $[B]$ array is well suited for inversion due to the normally large diagonal array representing the target element resistance values.

The eigenvalues consist of one set of complex conjugate values representing the oscillatory behavior of the basic *RLC* circuit, and the remaining eigenvalues are simple exponential decay functions. The oscillatory electrical frequency and damping are important parameters applicable to mechanical design. This solution prevails until the capacitor voltage reaches zero or clamps on a prescribed negative voltage. The values of the coil and target currents at this condition become the initial values for a second reduced-order eigensolution with the capacitor voltage removed from the state equations. The eigenvalues for this second *RL* circuit solution are, of course, all real exponential decay functions.

Comparison with Other Published Theoretical Solutions

The discrete element technique was utilized on the same problem that Henderson[3] solved by a totally different approach that employed Fourier-Hankel transformations. The problem specifications were as follows:

Coil: 0.25-in. inner diameter,
2.00-in. outer diameter,
0.188-in. thickness, 30 turns.
Gap: 0.0780 in.
Target: 0.0320-in. thickness,
conductivity 1.74×10^7 mhos/m.
Circuit: $C = 600\ \mu F$, $R_w = 0.084\ \Omega$,
$L_w = 23\ \mu H$, $V_o = 400$ V.

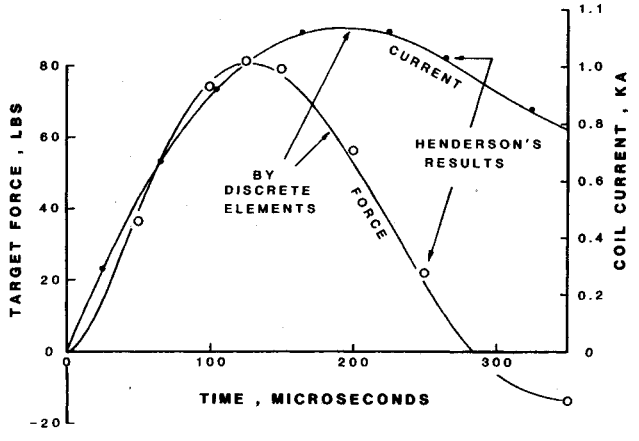

Fig. 5 Comparison of results from discrete element analysis with those calculated by Henderson.[3]

For the discrete element solution, the coil was divided into four segments and the target into four divisions in z and 20 divisions in r; $r = 0$–2.5 in. Substantial agreement by the two approaches is indicated by the plots shown in Fig. 5.

Lewis[2] reported values of mechanical impulse strength for the following set of parameters:

Coil: 4-mm inner diameter,
30-mm outer diameter,
2- and 5-mm thickness, 10 turns.
Gap: 2 mm.
Target: 1.0-mm thickness,
conductivity 2.5×10^7 mhos/m.
Circuit: Assumed analytical form

$$I = Ae^{-\alpha t}\sin(\omega t)$$

with α and ω listed in Table 1.

The identical analytical current was assumed for a discrete element solution. Lewis's published results were for specific impulse, and these results have been converted to actual impulse for purposes of comparison as displayed in Table 1. The agreement is observed to be within 1%.

Comparison with Published Experimental Results

Schrag[5] described a magnetic field measurement method for studying the distribution of eddy currents within and pressure distribution on a flat metallic plate subjected to a pulsed circular coil. This study was reviewed extensively by Henderson,[3] and various comparisons were made to the experimental data. The exceptionally close agreement between the discrete element solution and the work of Henderson was reported earlier, obviating the need for further comparisons.

Bernhart and Gien[4] described an experiment that employed a 48-in. length of polycarbonate rod that served to predict the temporal characteristics of the EIDI force pulse. They also made some attempt to correct their result for the effects of dispersion and attenuation. The problem specifications for this study are repeated as follows:

Coil: 0.245-in. inner diameter,
2.00-in. outer diameter,
0.135-in. thickness, 40 turns.
Gap: 0.080 in.
Target: 0.040-in. thickness,
conductivity 1.74×10^7 mhos/m.
Circuit: $C = 400\ \mu F$, $R_w = 0.0708\ \Omega$,
$L_w = 5.16\ \mu H$, $V_o = 1000$ V.

A comparison of the temporal force behavior is shown in Fig. 6.

Further numerical comparisons are presented in Table 2. The comparison is considered to be very favorable and evokes some confidence in the discrete element analysis procedure.

Example of Calculated Target Pressure

We now describe some calculated results for the following set of parameters:

Coil: 0.25-in. inner diameter,
2.00-in. outer diameter,
0.15-in. thickness, 29 turns.
Gap: 0.075 in.
Target: 0.065-in. thickness,
conductivity 1.74×10^7 mhos/m.
Circuit: $C = 100\ \mu F$, $R_w = 0.0\ \Omega$,
$L_w = 0.0\ \mu H$, $V_o = 1000$ V.

The coil was subdivided into six segments, and the target was assigned four divisions in z and 25 radial divisions, with a corresponding maximum radius of 2.5 in. Thus, the target to coil radius ratio is 2.5. The calculated normal force is depicted

in Fig. 7. It is typical of an impulse force applicable to deicing applications.

The pressure distributions were evaluated at the four distinct times shown in Fig. 7 and are displayed in Fig. 8. It may be observed that the pressure profile changes shape only slightly as time progresses.

The normal pressure calculated from Eq. (9) involves a summation of z-component forces on all of the target elements having the same radius. Figure 9 shows calculated data for the problem to which Figs. 7 and 8 apply. We show the force values for each of the four elements at the 0.6-in. radius position for the time $t = 50\ \mu$s. Two curves are shown, corresponding to the two radial flux densities expressed as the two separate terms in Eq. (6). We observe that the component of normal force coming from the radial flux density due to the target's eddy currents produces an expected "pinch effect" but negligible contribution to the total normal pressure.

Results with Multiple Coil Operation

To illustrate multiple coil analysis by the discrete element technique, the same parameters were used as listed in the pressure calculation example, except for capacitance and capacitor voltage. Impulse calculations were made for a fixed 50 J per coil and a fixed LC product for the circuit with $C = 200\ \mu F$ and $V_o = 707$ V selected for the single-coil case. With two series coils, C was halved and V_o doubled, etc. Under these conditions, the impulse strength should be independent of the number of coils used, provided the feed cables have no resistance. Calculated results shown in Fig. 10 show this to be true. However, when resistance is assigned to the cable, the results bear out the fact that series-connected coils are preferred.

Table 1 ($A = 1000$ A)

Coil thickness, mm	α, 1/s	ω, rad/s	Impulse, Lewis,[2] lb − s	Impulse, this paper, lb − s
2	7274.1	81020.5	0.0003392	0.0003379
5	3841.7	82741.2	0.0002725	0.0002717

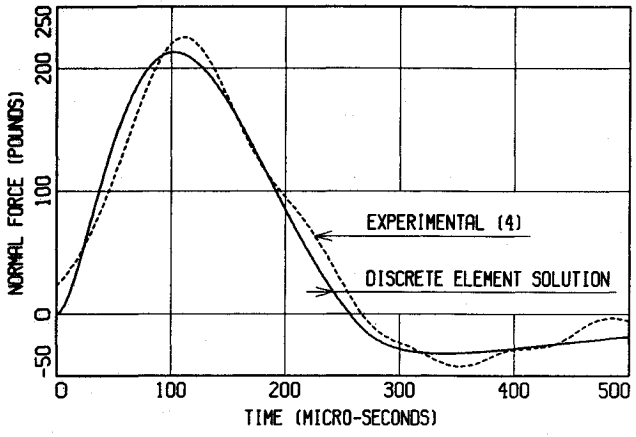

Fig. 6 Force comparison: discrete element analysis with Ref. 4.

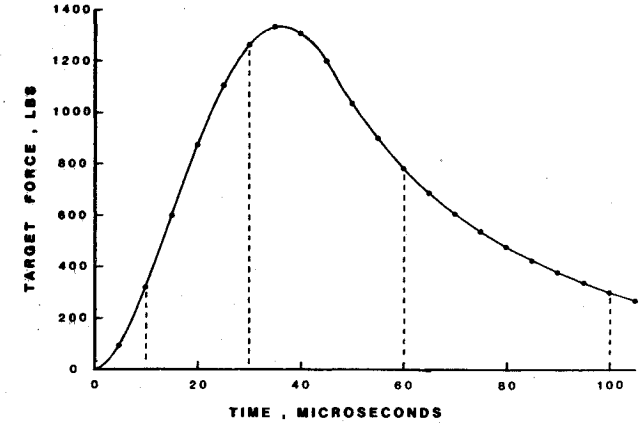

Fig. 7 Target force vs time.

Application to Nonrigid Targets

The intrinsic assumption in the discrete element method described by Eq. (13) is the notion of a stationary target and coil during the impulse period. This is contrary to the inherent concept of the EIDI system, which demands that the leading-edge skin (target) be expelled away from the pulsed coil.

When the electrical impulse period is excessive, the variable gap between the target and coil may influence not only the mechanical parameters but the electrical parameters as

Table 2 Numerical comparisons

Parameter	Experiment[4]	Discrete element analysis
Peak force, lb	225@112 μs	213@103 μs
Zero crossing	268 μs	257 μs
Impulse, lb − s	0.002000	0.002102

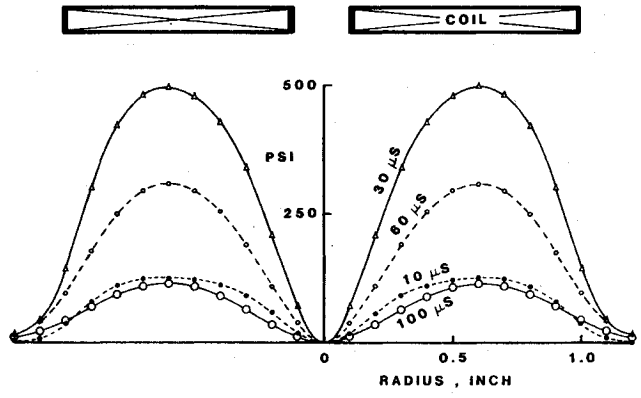

Fig. 8 Target pressure distributions.

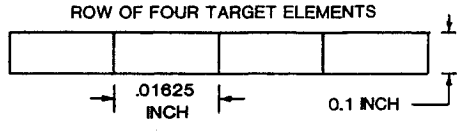

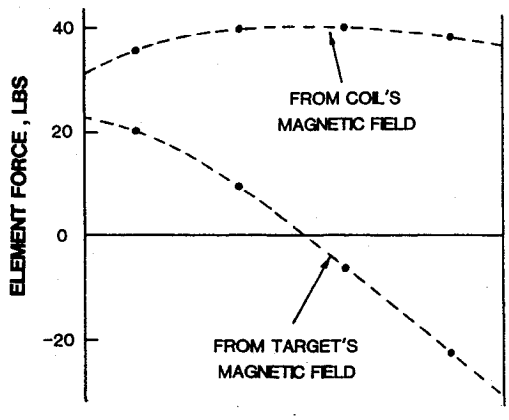

Fig. 9 Normal forces on target elements; $r = 0.6$ in., $t = 50\ \mu$s.

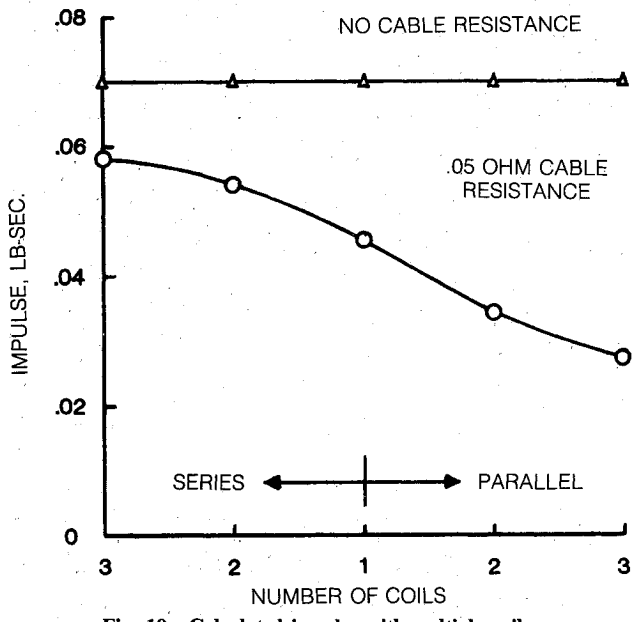

Fig. 10 Calculated impulse with multiple coils.

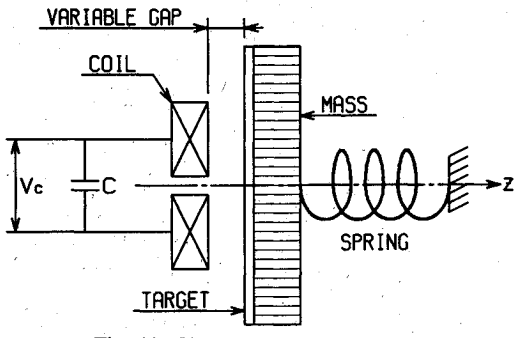

Fig. 11 Nonstationary target model.

well. A limited study of the nonstationary target problem was conducted by assuming a stationary coil and the target to be backed by a simple mechanical oscillator as shown in Fig. 11.

The most obvious change in the governing equations (13) is the requirement to account for the variable gap in the mutual inductance terms between the coil and target, i.e., submatrices $\{M_{TC}\}$ and $\{M_{CT}\}$. In addition, motional induction arising from the target velocity must be incorporated. Effects of both gap change and target velocity may be accounted for by generalizing the induction law to

$$\mathrm{d}[\{M(z)\}\{y\}]/\mathrm{d}t = \{M(z)\}\,\mathrm{d}\{y\}/\mathrm{d}t + \mathrm{d}\{M(z)\}/\mathrm{d}z(\mathrm{d}z/\mathrm{d}t)\{y\} \tag{16}$$

where $\mathrm{d}z/\mathrm{d}t$ is the target velocity and z is the longitudinal coordinate. Incorporating this modification into Eq. (13) for a single coil will yield

$$\begin{bmatrix} M_{TT} & M_{TC} & 0 \\ M_{CT} & M_{CC}+L_w & 0 \\ 0 & 0 & -C \end{bmatrix}\begin{Bmatrix} \dot{x} \\ \dot{y} \\ \dot{v}_c \end{Bmatrix} + \begin{bmatrix} \Delta R_T & \dot{z}M'_{TC} & 0 \\ \dot{z}M'_{CT} & R_w+\Delta R_c & (-1) \\ 0 & (-1) & 0 \end{bmatrix}\begin{Bmatrix} x \\ y \\ v_c \end{Bmatrix} = \begin{Bmatrix} 0 \\ 0 \\ -CV_0\delta(t) \end{Bmatrix} \tag{17}$$

where primes denote derivatives with respect to z.

The solution now becomes computationally intensive because both arrays $\{A\}$ and $\{B\}$ in Eq. (14) are time-dependent. It must be recognized that the time dependence is slowly varying such that the problem may be approximated by piecewise linear methods. A solution was obtained by Euler's method by using the following forward-difference approximation:

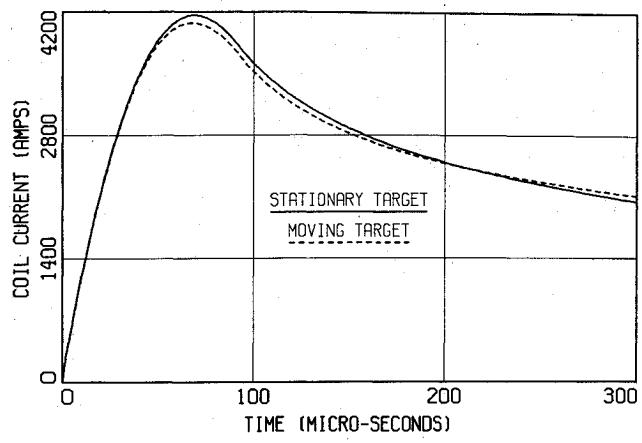

Fig. 12 Coil current comparison.

$$\mathrm{d}\{Z\}/\mathrm{d}t = \{[Z(t+\delta t)] - [Z(t)]\}/\delta t \tag{18}$$

The modified state model given by Eq. (14) would then have the form

$$\{Z(t+\delta t)\} = \{Z(t)\} + \{A^{-1}\}\{f(t) - [B(t)][Z(t)]\}\delta t \tag{19}$$

where $\{A^{-1}\}$ is the inverse of array $\{A\}$.

To minimize computational time and to control the quality of the required matrix inversion, the target was discretized into two z divisions and 12 radial divisions. The time-dependent subarrays $\{M_{TC}\}$ and $\{M'_{TC}\}$ were updated every two μs, and the value of δt, the numerical integration interval, was selected as 0.2 μs. The information related to the target gap and velocity is obtained from Newton's law applied to the mechanical oscillator. The mass of the target was selected as 0.0004 lb $-$ s^2/in., and the system was also modeled with a slight amount of damping ($\zeta = 0.02$). Two example problems were solved and are summarized next.

Example 1 Specifications

Coil: 0.25-in. inner diameter,
1.829-in. outer diameter,
0.150-in. thickness,
three segments, and 36 turns.
Gap: 0.075 in. (initial).
Target: 0.045-in. thickness,
conductivity 1.74×10^7 mhos/m.
Circuit: $C = 200\ \mu F$, $V_o = 1404.2$ V,
$L_w = 0$, $R_w = 0$.

The mechanical frequency was selected as 1400 Hz. The electrical frequency corresponding to the selected coil and target combination was 2776 Hz. This combination yields the following design relationship:

$$\frac{\text{Electrical frequency}}{\text{Mechanical frequency}} = 1.983 \tag{20}$$

Three figures comparing the computed results for the stationary and moving target cases are shown. Figure 12 shows the negligible effects on the coil current trace, Fig. 13 depicts the slight degradation in the normal (EIDI) force, and Fig. 14 is the resulting gap comparison. In the latter figure, the "stationary target" means the gap derived from the stationary target force.

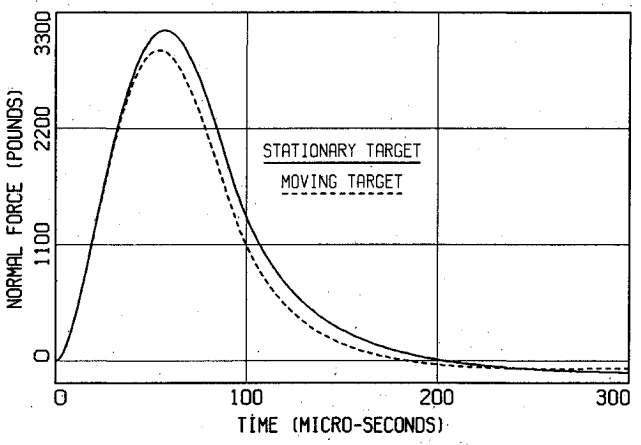

Fig. 13 Normal force comparison.

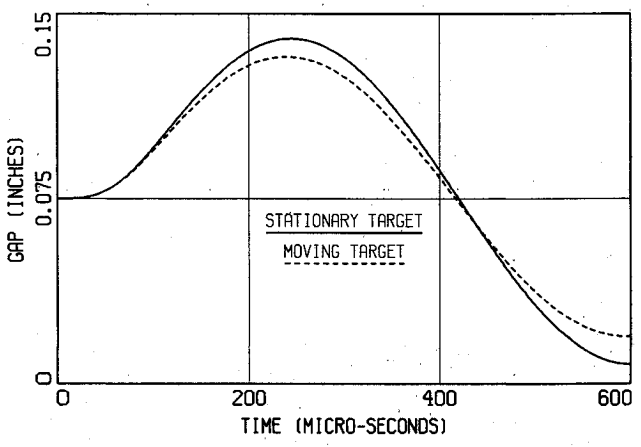

Fig. 14 Gap comparison.

As can be noted from these figures, the target dynamics is only mildly affected by the moving target analysis.

Example 2 Specifications

Coil: 0.25-in. inner diameter,
2.445-in. outer diameter,
0.150-in. thickness,
three segments, and 50 turns.
Gap: 0.075 in. (initial).
Target: 0.045-in. thickness,
conductivity 1.74×10^7 mhos/m.
Circuit: $C = 600\ \mu F$, $V_o = 1700$ V,
$L_w = 0$, $R_w = 0$.

The mechanical frequency was selected as 3200 Hz. The selected coil and target combination for this example yields an electrical frequency of 871 Hz and the following frequency ratio:

$$\frac{\text{Electrical frequency}}{\text{Mechanical frequency}} = 0.272 \qquad (21)$$

Three figures comparing the computed results for the stationary and moving cases are again shown. Figure 15 shows the effects on the coil current trace. Figure 16 is a display of the normal (EIDI) force for both the stationary and moving target, as well as a third curve that includes the inductance changes arising from the gap changes but neglects the motional induction effects. Obviously, motional induction is an important contributing factor. Figure 17 is a display of the changes in the gap. The peak gap reduction of 25% is attributed to the target force pulse duration, which is of the same order as the mechanical period, 312.5 μs.

We would conclude from these two examples that the EIDI design guide, of selecting the electrical frequency about twice

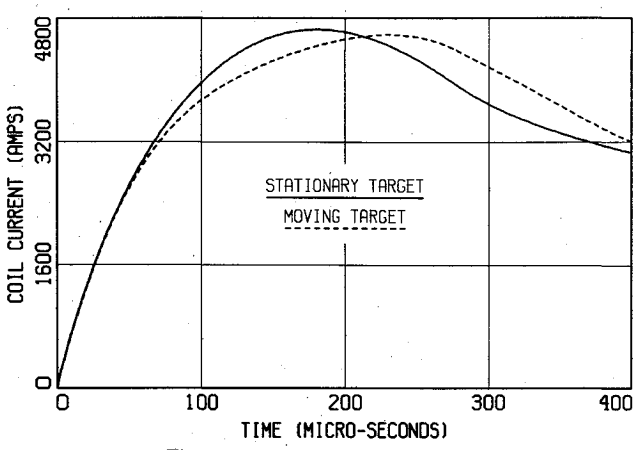

Fig. 15 Coil current comparison.

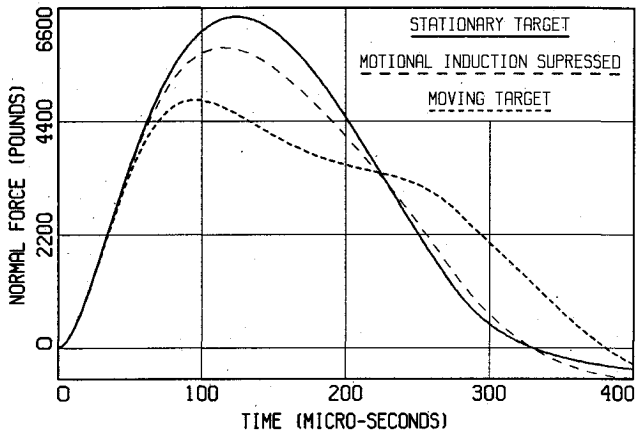

Fig. 16 Normal force comparison.

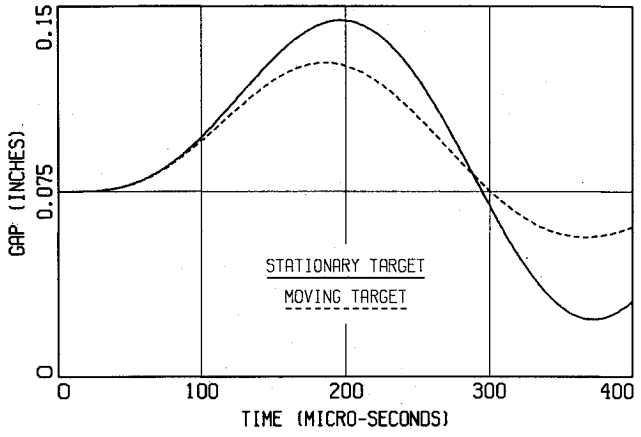

Fig. 17 Gap comparison.

that of the mechanical frequency, is sound. When this condition is satisfied, the error in determining the structural dynamic response from stationary target force and pressure calculations is small.

Comments on Discretizing the Coil and Target

Decisions on the number of coil segments and discrete target elements to use are based on acceptable compromises between accuracy and computation time. The time required is substantially dictated by the total system order as given by Eq. (15). In this equation, it will be recalled that N_C represents the number of coil segments. This typically ranges from 1 to 6 and so does not contribute significantly to the system order. On the other hand, N_T, the number of discrete target

elements, may range from 10 to 150. The axial dimension of a target element is established by subdividing the target thickness into 2–6 equal divisions, and the radial dimension by assigning 5–25 equal radial divisions from the z axis to approximately 2–2.5 times the coil radius. It has also proved expedient to simulate a small hole in the center of the target, which serves to obviate numerical problems identified with a zero radius.

Depending on the goal of the calculations, good results may be obtained with relatively low system order. For example, in the moving target study, one set of calculations was made with the target blocked. Comparing results for system orders of 28 and 107 showed agreements to within 2% for both coil currents and total normal target forces. Thus, for circuit studies, including predictions of the oscillatory frequency and damping as well as current and voltage behavior, a total order of 12–20 is probably adequate. Low orders are also useful for conducting computational searches to establish coil designs that will yield desired force pulse durations and/or impulse strengths.

In contrast, accurate results on the distribution of target pressure require a large number of target elements. The pressure distributions shown in Fig. 8 were calculated using 80 target elements. Similarly, special studies on the process of magnetic energy diffusion in the coil call for a larger number of coil segments.

Conclusions

The goal of this research was to develop a time-domain computational procedure that would economically provide the following information associated with an EIDI pulse:

1) Detailed normal and radial pressure distributions.
2) Normal target force; peak value, zero crossing, and impulse strength.
3) Current diffusion through the coil and target.
4) Circuit voltage and current traces.

The noted comparisons demonstrate very good agreement with other published theoretical solutions and experimental results. Thus, the remaining question is associated with the computational efficiency.

The computer code is currently operating on an IBM-3081 large-scale system and requires a core size of 1400 kilobytes, which is quite modest by 1987 standards. Execution times run from a few seconds to approximately 3 min. These time variations are associated with the problem size specification discussed earlier. It is also noteworthy to mention that the digital code is used to predict the electrical frequency parameter used in mechanical design applications. This function has been assigned to a 640K microcomputer, further dramatizing the simplicity and speed of the time-domain discrete element solution.

Acknowledgments

This study has been funded in part by the NASA Lewis Research Center under Grant NAG-3-284. The authors also wish to extend their appreciation to Mr. Peter H. Gien for his assistance.

References

[1]Bowley, R. M., King, P. J., Lewis, G. J., and Shellard, I., "Production of Short Mechanical Impulses by Means of Eddy Currents," *Proceedings of the IEE*, Vol. 130, No. 6, Part B, Nov. 1983, pp. 415–423.

[2]Lewis, G. J., "The Electrodynamic Operation of Electro-Impulse De-Icing Systems," AIAA Paper 86-0547, Jan. 1986.

[3]Henderson, R. A., "Theoretical Analysis of the Electrical Aspects of the Basic Electro-Impulse Problem in Aircraft De-Icing Applications," Ph.D. Thesis, Wichita State University, Wichita, KS, March 1986.

[4]Bernhart, W. D. and Gien, P. H., "A Structural Dynamics Investigation Related to EIDI Applications," AIAA Paper 86-0550, Jan. 1986.

[5]Zumwalt, G. W., Schrag, R. L., Bernhart, W. D., and Friedberg, R. A., "Analysis and Tests for Design of an Electro-Impulse De-Icing System," NASA Contractor Rept. 174919, May 1985, pp. 42–74.